A SEARCH FOR UNTRIGGERED GRB AFTERGLOWS WITH ROTSE-III

E. S. Rykoff,[1] F. Aharonian,[2] C. W. Akerlof,[1] K. Alatalo,[1] M. C. B. Ashley,[3] T. Güver,[4] D. Horns,[2] R. L. Kehoe,[5]
Ü. Kiziloğlu,[6] T. A. McKay,[1] M. Özel,[7] A. Phillips,[3] R. M. Quimby,[8] B. E. Schaefer,[9] D. A. Smith,[1]
H. F. Swan,[1] W. T. Vestrand,[10] J. C. Wheeler,[8] J. Wren,[10] AND S. A. Yost[1]

ABSTRACT

We present the results of a search for untriggered gamma-ray burst (GRB) afterglows with the Robotic Optical Transient Search Experiment-III (ROTSE-III) telescope array. This search covers observations from 2003 September to 2005 March. We have an effective coverage of 1.74 deg^2 yr for rapidly fading transients that remain brighter than ~17.5 mag for more than 30 minutes. This search is the first large-area survey to be able to detect typical untriggered GRB afterglows. Our background rate is very low and purely astrophysical. We have found four previously unknown cataclysmic variables (CVs) and one new flare star. We have not detected any candidate afterglow events or other unidentified transients. We can place an upper limit on the rate of fading optical transients with quiescent counterparts dimmer than ~20th magnitude at a rate of less than 1.9 deg^{-2} yr^{-1} with 95% confidence. This places limits on the optical characteristics of off-axis (orphan) GRB afterglows. As a by-product of this search, we have an effective ~52 deg^2 yr of coverage for very slowly decaying transients, such as CVs. This implies an overall rate of outbursts from high Galactic latitude CVs of 0.1 deg^{-2} yr^{-1}.

Subject headings: galaxies: active — gamma rays: bursts — novae, cataclysmic variables

1. INTRODUCTION

There is much circumstantial evidence that gamma-ray burst (GRB) outflows are highly relativistic and collimated. An achromatic break has been seen in light curves for several GRB afterglows, with the canonical example being GRB 990510 (Harrison et al. 1999; Stanek et al. 1999). These breaks are naturally explained by a geometric constraint on the outflow. The jet opening angle has been inferred for GRB 990510 and several other GRBs and appears to range from 2° to 30° (Frail et al. 2001; Panaitescu & Kumar 2001). Therefore, the true rate of GRBs must be ≳100 times that detected by satellite experiments such as the Burst and Transient Source Experiment (BATSE), the *High Energy Transient Explorer-2* (*HETE-2*), *the International Gamma-Ray Astrophysics Laboratory* (*INTEGRAL*), and *Swift*. Although the Earth will not receive γ-ray emission from these bursts, they might be detectable at longer wavelengths. It remains an open question what these off-axis "orphan" afterglows should look like. In the simplest model, an orphan afterglow looks like a standard afterglow, except that it becomes visible after a delay of ~0.5 day. As the ejecta cools, the relativistic beaming angle increases until the afterglow can be seen off-axis, long after the γ-rays have ceased (Rhoads 1997). However, this assumes that there is no significant optical emission outside the γ-ray beaming angle. Nakar & Piran (2003) have suggested that the beaming angle of the optical emission might be different from that of the γ-ray emission. They refer to these afterglows as "on-axis orphan afterglows." A detectable rate of orphan afterglows gives an orthogonal approach to measuring typical GRB collimation.

Whether or not orphan (off-axis) afterglows are detectable, there must be untriggered afterglows from normal GRBs that simply have not been seen by a γ-ray satellite. *Swift* can detect approximately two GRBs per week in its field of view, while an extrapolation of the BATSE event trigger rate for the entire sky suggests that there are approximately two GRBs per day visible to the Earth, corresponding to 0.018 deg^{-2} yr^{-1} (Fenimore et al. 1993). How much solid angle would a survey need to cover to observe an untriggered GRB afterglow serendipitously? We know from the Robotic Optical Transient Search Experiment-I (ROTSE-I) and Livermore Optical Transient Imaging System (LOTIS) prompt follow-ups to BATSE triggers that the preponderance of early afterglows do not get as bright as 14th magnitude (Akerlof et al. 2000; Kehoe et al. 2001; Park et al. 1999). Currently, we do not have enough data on early afterglows with deeper imaging to provide any firm predictions of the rate of detectable bursts. We expect this to change now that *Swift* is operational. Rapid follow-up to a small number of *HETE-2* triggers has shown that approximately 50% of bursts might be brighter than ~18.5 for 30 minutes or more (Lamb et al. 2004). Thus, around 9×10^{-3} bursts deg^{-2} yr^{-1} should be visible to an instrument capable of reaching this magnitude, such as ROTSE-III. Thus, an exposure of ~110 deg^2 yr is required for a high probability of finding an afterglow independent of any γ-ray trigger.

To date, there have only been a few published searches for untriggered and orphan GRBs and other short-duration transients. These searches have all probed different magnitude ranges and

[1] Physics Department, University of Michigan, 2477 Randall Laboratory, 450 Church Street, Ann Arbor, MI 48109-1040; erykoff@umich.edu, akerlof@umich.edu, kalatalo@umich.edu, tamckay@umich.edu, donaldas@umich.edu, hswan@umich.edu, sayost@umich.edu.

[2] Max-Planck-Institut für Kernphysik, Saupfercheckweg 1, 69117 Heidelberg, Germany; felix.aharonian@mpi-hd.mpg.de, horns@mpi-hd.mpg.de.

[3] School of Physics, Department of Astrophysics and Optics, University of New South Wales, Sydney, NSW 2052, Australia; mcba@phys.unsw.edu.au, a.phillips@unsw.edu.au.

[4] Istanbul University Science Faculty, Department of Astronomy and Space Sciences, 34119, University-Istanbul, Turkey; tolga@istanbul.edu.tr.

[5] Department of Physics, Southern Methodist University, Dallas, TX 75275; kehoe@physics.smu.edu.

[6] Department of Physics, Middle East Technical University, Ankara 06531, Turkey; umk@astroa.physics.metu.edu.tr.

[7] Department of Physics, Çanakkale Onsekiz Mart Üniversitesi, Terzioğlu 17020, Çanakkale, Turkey; me_ozel@ibu.edu.tr.

[8] Department of Astronomy, University of Texas, Austin, TX 78712; quimby@astro.as.utexas.edu, wheel@astro.as.utexas.edu.

[9] Department of Physics and Astronomy, Louisiana State University, Baton Rouge, LA 70803; schaefer@lsu.edu.

[10] Los Alamos National Laboratory, NIS-2, MS-D436, Los Alamos, NM 87545; vestrand@lanl.gov, jwren@nis.lanl.gov.

timescales. In general, a wide-field instrument can cover a wider solid angle but cannot go very deep. The ROTSE-I transient search covered 3.5 deg^2 yr, to a limiting magnitude of 15.7 (Kehoe et al. 2002). The Rapid Telescopes for Optical Response (RAPTOR) array covers the entire visible sky several times each night to a limiting magnitude of 12 and is sensitive to very fast transients, on the order of minutes (Vestrand et al. 2004). The Deep Lens Survey (DLS) transient search covered 0.01 deg^2 yr with sensitivity to 24th magnitude and found a couple of tantalizing unidentified transients (Becker et al. 2004). In spite of the relatively rapid detection of these transients, they were too faint for spectroscopic follow-up and could not be positively identified as extragalactic or associated with GRBs. Vanden Berk et al. (2002) performed a color-selected transient search with the Sloan Digital Sky Survey (SDSS) to a limiting magnitude of 19 and detected one unusual active galactic nucleus (AGN).

The search reported in this paper was specifically designed to detect untriggered and orphan GRB afterglows. This search is based on the assumption that an orphan afterglow might have an optical behavior similar to that of observed afterglows. As a result, we search for transients that meet two criteria: first, the quiescent counterpart or host galaxy would have $m_R > 20$ and would not be detectable by ROTSE-III; and second, the transient must be brighter than our limiting magnitude for at least 30 minutes. Other known astrophysical sources fall into this category, including: cataclysmic variables (CVs) and novae in the Galactic halo that burst by >2 mag; faint flare stars that brighten on short timescales by several magnitudes; and AGNs, blazars, and quasars that display optically violent variability (OVV), occasionally flaring by several magnitudes on very short timescales.

The rapid identification of new transients is essential for a search of this nature. Only spectroscopic follow-up can positively identify an orphan afterglow or a new type of astrophysical phenomenon. As ROTSE-III can identify transients while they are still relatively bright, this enables follow-up with telescopes with modest apertures.

2. OBSERVATIONS AND DATA REDUCTION

The ROTSE-III systems are described in detail in Akerlof et al. (2003). The ROTSE-III telescopes are installed at four sites around the globe: Coonabarabran, Australia; Fort Davis, Texas; Mount Gamsberg, Namibia; and Bakirlitepe, Turkey. They have a wide ($1°.85 \times 1°.85$) field of view imaged onto an E2V 2048×2048 back-illuminated, thinned CCD, and they operate without filters. The camera has a fast readout cycle of 6 s. The limiting magnitude for a typical 60 s exposure is around $m_R \sim 18.5$, which is well suited for the study of GRB afterglows during the first hour or more. The typical FWHM of the stellar images is <2.5 pixels (8″.1).

In 2003 September we initiated analysis of our nightly sky patrol images for rapid identification of fast transients. The region patrolled includes 370×3.4 deg^2 fields in the equatorial stripe with declination of $|\delta| < 2°.64$. To avoid field crowding and Galactic opacity, all the fields are at high Galactic latitude with $|b| > 30°$. Because asteroids were a significant background early in our search, after 2004 May we only imaged fields with ecliptic latitudes of $|\beta| > 10°$. These fields were chosen for two primary reasons. First of all, they are visible to all four ROTSE-III locations, two of which are in the northern hemisphere and two of which are in the southern hemisphere. Furthermore, this region has public SDSS data with five-color imaging to well below our limiting magnitude (Abazajian et al. 2005). This allows calibration of our fields to a set of well-

measured stars, as well as providing easy identification of flares from objects such as CVs and quasars.

Our standard observing sequence includes a pair of closely spaced 60 s exposures, followed after 30 minutes by a second pair of 60 s exposures. We define a *set* of images as four consecutive images taken with this interval. The second image of each pair is offset by ∼10 pixels to reduce the impact of bad pixels. During bright moon conditions (lunar illumination >70%), we reduce the exposure length to 20 s to prevent the background sky from saturating the images. The 30 minute interval was chosen to enhance sensitivity to rapidly fading transients while still allowing a large solid angle coverage.

After each image is recorded, it is dark-subtracted and flat-fielded by an automated pipeline. Twilight flats are generated every night and are updated for the pipeline on a monthly basis. Our back-illuminated thinned CCD imager, combined with broadband filterless optics, consequently imposes an interference fringe pattern on all images. We therefore must correct for these fringing effects. The pattern is stable, although the amplitude varies with the brightness of night-sky lines. We have created a fringe map for each CCD by comparing a twilight flat image, which does not display a fringe pattern, with a sky flat image, which does display a fringe pattern. After flat fielding, the sky pixels in the central subregion of the image are fitted via linear regression with the corresponding pixels in the fringe pattern. The fringe pattern is then scaled accordingly and subtracted from the image. If the fit is poor (reduced $\chi^2 > 3$), due to scattered moonlight or clouds in the image, the fringe pattern is not subtracted. In the worst case, the fringe pattern can introduce photometric errors as large as 5% and can produce occasional false detections of faint objects.

The pipeline then runs SExtractor (Bertin & Arnouts 1996) to perform initial object detection, measure centroid positions, and determine aperture magnitudes. A separate pipeline program written in IDL (`idlpacman`) correlates the object list with stars brighter than 15th magnitude in the United States Naval Observatory A2.0 (USNO-A2.0) catalog to determine an astrometric solution as well as an approximate magnitude zero point for the field.

The limiting magnitude of each image is estimated from the background noise, FWHM of the point-spread function (PSF), and the zero-point offset, which is essentially a measure of the transparency of the sky. With these three values, we can estimate the magnitude at which we can detect a star 90% of the time with our SExtractor cuts in an uncrowded region of sky. As shown in § 3, our detection efficiency declines very rapidly in crowded regions.

After each pair of images is calibrated, we pair-match the object lists. Objects that are detected in both of the pair of images are considered real. All objects that are detected only in a single image are rejected. This strategy removes most spurious detections caused by cosmic rays, pixel defects, satellite glints, and noise spikes. However, some backgrounds still remain: noise spikes usually due to imperfect fringe subtraction when the sky is not fully transparent, some cosmic-ray coincidences, and asteroids.

One of the great difficulties in calibrating a large-area survey of this type is the lack of standard stars uniformly distributed across the sky. The USNO-A2.0 catalog provides excellent astrometric solutions for any field, as there are typically >1000 stars with $R < 15$. However, the photometric zero points as determined from USNO-A2.0 R-band magnitudes have typical systematic errors of up to 0.30 mag (Monet et al. 1998), making field-to-field comparisons difficult.

For around 90% of our fields, we have significant overlap with SDSS five-color data. We have thus decided to recalibrate all of our fields relative to the SDSS r' band, as the field-to-field
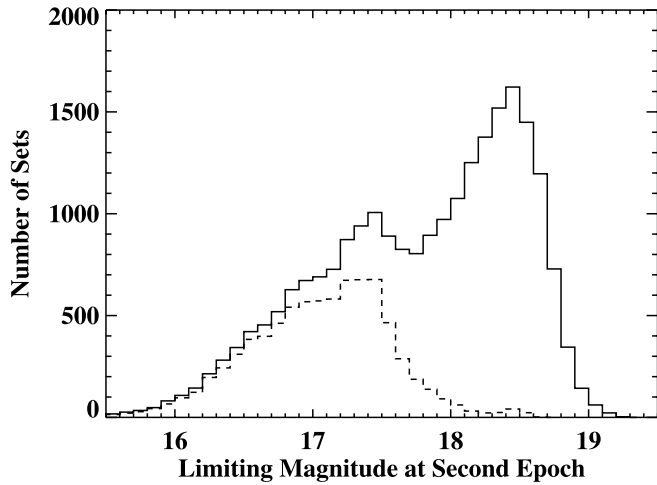
FIG. 1.—Histogram of number of sets searched as a function of limiting magnitude [$m_{\mathrm{ROTSE\,(SDSS)}}$] at the second (return) epoch. The limiting magnitude at the second epoch is the primary constraint for detecting quickly fading transients. The solid histogram describes all sets imaged, and the dashed histogram describes the contribution from 20 s exposures taken during bright lunar phases.

variations are around 2% (Abazajian et al. 2005). For each of our overlapping fields, we compare all ROTSE-III template stars that have counterparts in SDSS between $15 < r' < 17$ with $g' - r' < 1.0$. We find that the typical offset is 0.22 ± 0.16 when converting from $m_{\mathrm{ROTSE\,(USNO)}}$ to $m_{\mathrm{ROTSE\,(SDSS)}}$. The scatter in offsets is primarily due to systematic errors in the USNO-A2.0 R-band zero points. For the remaining $\sim$10% of sky patrol fields without SDSS calibration data, we have offset the zero points obtained from USNO-A2.0 calibration by 0.22 mag. For the remainder of this paper, the magnitudes quoted are calibrated relative to the SDSS r' band.

Through 2005 March we have searched over 23,000 sets of images for new transients as described in § 1. Figure 1 is a histogram of the number of sets searched as a function of limiting magnitude at the second (return) epoch. Since we demand that a new transient be present in an entire set, the limiting magnitude at the second epoch is the primary constraint for detecting rapidly fading transients. The solid histogram describes all sets imaged, and the dashed histogram describes the contribution from 20 s exposures taken during bright lunar phases.

3. ANALYSIS

We have chosen to identify transients by the appearance of a new object compared to a template list of ROTSE-III objects. This strategy has distinct advantages for our survey relative to image subtraction. As most of our fields are relatively uncrowded, we only lose $\sim$4% of our solid angle to direct starlight. Due to bandwidth limitations at our remote observatory sites, we need a strategy that is fast and has relatively few false positives. Image subtraction routines are very sensitive to variations in PSF that are difficult to keep absolutely steady in an automated telescope over a wide range of conditions. Finally, as shown below, our solid angle efficiency is over 80% for detection of transients in most of our high Galactic latitude fields, comparable to the search strategy employed by the DLS (Becker et al. 2004).

Our basic detection algorithm is quite simple. We demand that a new object is detected in at least four consecutive images, or an entire set. The position resolution of each of the images must be less than 0.3 pixels (1″). This removes images that are out of focus and images with anomalously large PSFs common on windy nights. The new object must be more than 5 pixels (16″.2)

from the nearest ROTSE-III template object. We have no cuts on the shape of the light curve so as not to limit the types of transient we can detect, although we do demand that the brightest detection is brighter than 18th magnitude. For each candidate we examine its PSF to ensure that it is comparable to the PSF of its neighbors. We next place an aperture at the same location in two of our best template images to check if there is an object that had not been properly deblended by SExtractor.

After these cuts have been performed, typically $\ll$1 transient remains in each set. Occasionally there are more detections, usually due to instrumental effects such as artifacts near saturated stars, or due to deblending problems caused by bad focus or wind-degraded images. Therefore, if more than five transient candidates remain in a set, then it is rejected as a bad set.

Thumbnail images of the remaining transient candidates are then copied to a Web site at the University of Michigan for hand scanning. These candidates are usually faint stars that are just at our detection threshold and that are clearly visible in the Multimission Archive at STScI Digitized Sky Survey (MAST DSS; Lasker et al. 1998). Occasionally there is a minor planet near opposition that has a proper motion of $<1''$ during the 30 minute interval between exposure pairs. These minor planets are usually in the Minor Planet Center MPChecker database, allowing easy exclusion.

In order to measure our overall efficiency, we must be able to parameterize our coverage for each field. We have used typical test fields to estimate the detection efficiency as a function of distance to the nearest template star and thus derive the effective solid angle covered for each of our sky patrol fields. We can also calculate the probability of detecting a transient relative to the limiting magnitude of the field.

Figure 2 shows the detection efficiency as a function of distance to the nearest template star. To obtain this plot we ran a Monte Carlo simulation; 50,000 objects were uniformly distributed in magnitude from 10.0 to 19.0 at random positions in a pair of sample images. The objects were generated with the IDL astronomy library function `psf_gaussian`, with the median FWHM of a star in the field. We then added the pixel counts at the appropriate positions in the image. These new images were reprocessed in the standard analysis pipeline. Only simulated objects that were detected in each of the pair of images were
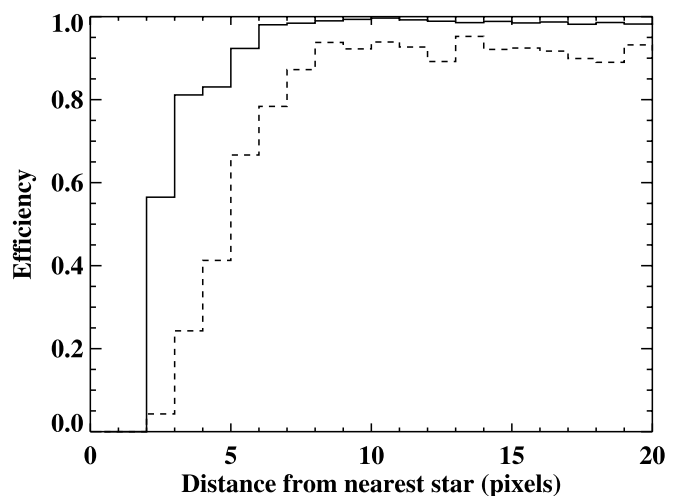

FIG. 2.—Detection efficiency in a pair of images vs. distance from nearest template star. The solid line describes simulated objects more than 0.5 mag brighter than the limiting magnitude; the dashed line describes simulated objects within 0.5 mag of the limiting magnitude, where our detection efficiency is reduced.
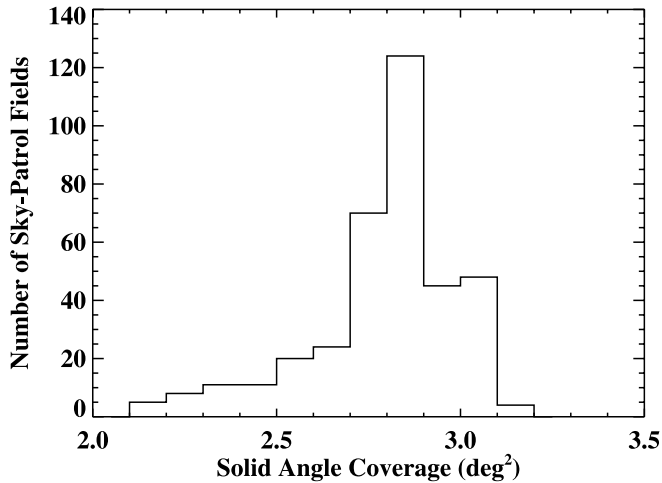
FIG. 3.—Histogram of solid angle coverage for our sky patrol fields. The maximum available solid angle in our field is 3.42 deg^2, and the efficiency in most of the fields is >80%.

considered. For this plot, any object that is within 2 pixels of a template star is vetoed; in our actual search we place the cut at 5 pixels, which incurs a minimal penalty in solid angle coverage while greatly decreasing the number of false detections from deblending issues. The solid histogram describes simulated objects more than 0.5 mag brighter than the limiting magnitude. The dashed histogram describes simulated objects within 0.5 mag of the limiting magnitude, where the detection efficiency is reduced by ~20%.

Figure 3 shows a histogram of the available solid angle coverage for each of our sky patrol fields. To determine these values, we calculated the distance from each pixel to the nearest template star in each field. The solid angle lost in each field is primarily due to the 5 pixel exclusion radius around each template star. Additional pixels are masked out in the wings of very bright stars and saturation bleed trails from bright stars. These typically cover ~1% of each field. In most of our fields the efficiency is greater than 80%. The low-coverage tail comprises dense fields including those containing globular clusters.

4. RESULTS

4.1. Transient Detections

Through 2005 March, we have found four new cataclysmic variables and one flare star. This is a comprehensive list of all of our transient detections that were not identified as asteroids. Each of these objects was well below our detection limits in quiescence. A brief description of these objects follows.

CV ROTSE3 J151453.6+020934.2.—This CV was detected by ROTSE-IIIb on 2004 March 28, at 16th magnitude, over 3 mag brighter than quiescence. It remained around 17th magnitude for 2 weeks before fading below our detection threshold. During quiescence we obtained *UBVI* measurements from the MDM Hiltner 2.4 m telescope on Kitt Peak, Arizona. Its colors were consistent with a dwarf nova at minimum light (Rykoff et al. 2004a).

CV ROTSE3 J221519.8−003257.2.—This CV was detected by ROTSE-IIId on 2004 July 8, at 17.5th magnitude, around 3 mag brighter than quiescence. The outburst lasted over 2 days before fading below our detection threshold. As with the previous CV, its colors during quiescence were consistent with a dwarf nova at minimum light (Rykoff et al. 2004a). This CV burst

again on 2004 October 4. It was detected by ROTSE-IIId at 17.2 mag and was again discovered by our transient detection pipeline.

Flare star ROTSE3 J220806.9+023100.3.—This flare star was detected by ROTSE-IIIb on 2004 November 12, at 16th magnitude. It faded by 0.8 mag in 30 minutes, mimicking our expected signature of an untriggered GRB afterglow. However, the counterpart was clearly visible in the Two Micron All Sky Survey at $J \sim 15$. In addition, the $J - H$ and $H - K$ colors of 0.65 and 0.32, respectively, suggest a very red object. Finally, the USNO-B1.0 catalog measured proper motion of the quiescent counterpart of 32 mas yr^{-1}. These observations are consistent with a flare from a nearby M dwarf–type star.

CV 2QZ J142701.6−012310.—This CV was detected by ROTSE-IIIc on 2005 January 23, at 15th magnitude, around 5 mag brighter than quiescence. It remained bright around 16th magnitude for about 7 days before fading below our detection threshold. A spectrum previously had been obtained during quiescence by the Two Degree Field (2dF) redshift survey. In addition, a spectrum of the object during outburst was obtained by the Hobby-Eberly Telescope (HET) at McDonald Observatory on January 25, which showed a blue continuum with no obvious emission or absorption features (Rykoff 2005). Follow-up observations of the object during quiescence at the University of Cape Town revealed this to be a rare Am CVn type, doubly degenerate helium transferring binary (Woudt et al. 2005).

CV ROTSE3 J100932.2−020155.—This CV was detected by ROTSE-IIIc on 2005 February 20, at 14th magnitude, around 6 mag brighter than quiescence. It faded slowly over the next 27 days before dropping below our detection threshold. Two spectra had previously been obtained during quiescence by the 2dF redshift survey. A spectrum from the HET on 21 February displays prominent Hα emission expected from a CV, and the object is consistent with a SU UMa dwarf nova during a super outburst (Rykoff & Quimby 2005).

4.2. Transient Detection Efficiency

We calculate our detection efficiency using different methods for two different types of transients. The first method is suitable for slowly decaying transients such as cataclysmic variables and other novae that rise rapidly and are roughly constant over our observation interval. These objects typically stay brighter than our limiting magnitude for over 1 day. Our effective time coverage for these transients is therefore quite high.

In the second method, suitable for short-duration (rapidly fading) transients, we parameterize the transients as GRB afterglows with a simple decaying power law. This determines our sensitivity to rapidly varying transients but describes a relatively small effective time coverage. Specifically, the time that the transient is brighter than our limiting magnitude must be >30 minutes.

To calculate our sensitivity for slowly decaying transients, we examine the limiting magnitudes of each set of images. First, we account for the solid angle covered, as plotted in Figure 3. We then generate 5000 simulated transients uniformly distributed from 9.5th to 20th magnitude. If an object is >0.5 mag brighter than the limiting magnitude in an individual image, it is considered a detection. If it is <0.5 mag brighter than the limiting magnitude, there is a 90% chance that it will be detected. An object must be detected in all four of a set of images, and at least one detection must be brighter than $m_{ROTSE} = 18.0$. This decreases our efficiency for faint CVs, but it also greatly decreases the false detections as well as simplifying the interpretation of the data.
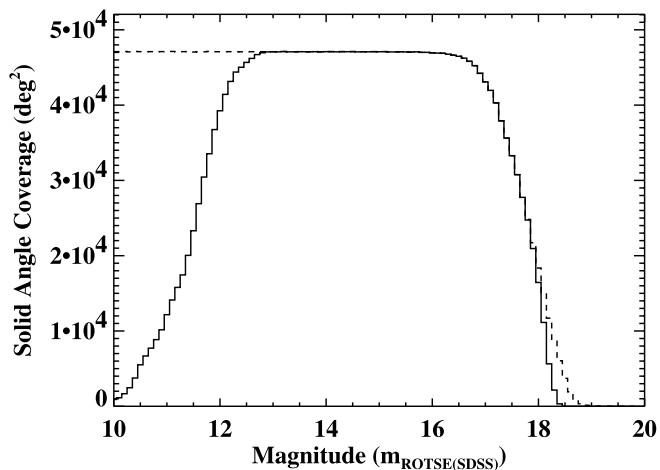
FIG. 4.—Histogram of total solid angle coverage for new slowly decaying sources. The solid histogram describes objects that pass our cuts. The dashed histogram describes objects that are detected but do not pass our cuts, either due to saturation at the bright end or due to falling below our magnitude threshold.

Figure 4 shows our total solid angle coverage for new slowly decaying sources. The detection efficiency before cuts is shown with the dashed histogram. After we apply saturation cuts and our magnitude cut, the result is the solid histogram. This plot was made using all of our sets with limiting magnitudes deeper

than $\sim$17, with over 47,000 deg^2 of coverage. For transients that remain roughly constant for over 0.5 days, this results in $\sim$52 deg^2 yr of coverage for CVs that peak between 13th and 16th magnitude.

To calculate our sensitivity to short-duration transients, we parameterize each transient as a fading power law, $f = f_0 t^{-\alpha}$. Each transient is assigned a peak magnitude, m_{60}, at $t = t_0 + 60$ s and a decay constant α. The effective coverage time for each set is the time period when a transient outburst would be detected in our search. We have decided to assume an effective coverage time of 30 minutes for each set of four observations, although our efficiency depends on peak magnitude and decay constant for each transient. The effective coverage time refers to the *preceding* 30 minute interval, as our search is insensitive to transients that appear between our two observation epochs. In order to achieve $\sim$100% efficiency for a transient type in our observation window, it must remain above our limiting magnitude for at least 1 hr.

As before with slowly decaying transients, we first account for the solid angle covered in each field. We ran a Monte Carlo simulation with 5000 objects per set. The peak magnitude m_{60} was uniformly distributed from 7.5 to 18.5, the decay constant α was uniformly distributed from 0.3 to 2.5, and the burst time t_0 was set at a random time at most 30 minutes *prior* to the first image in the set. Essentially, we are calculating the detection efficiency when assuming that our coverage time is 30 minutes for each set. As mentioned above, objects <0.5 mag brighter than the limiting magnitude have a 90% chance of detection.
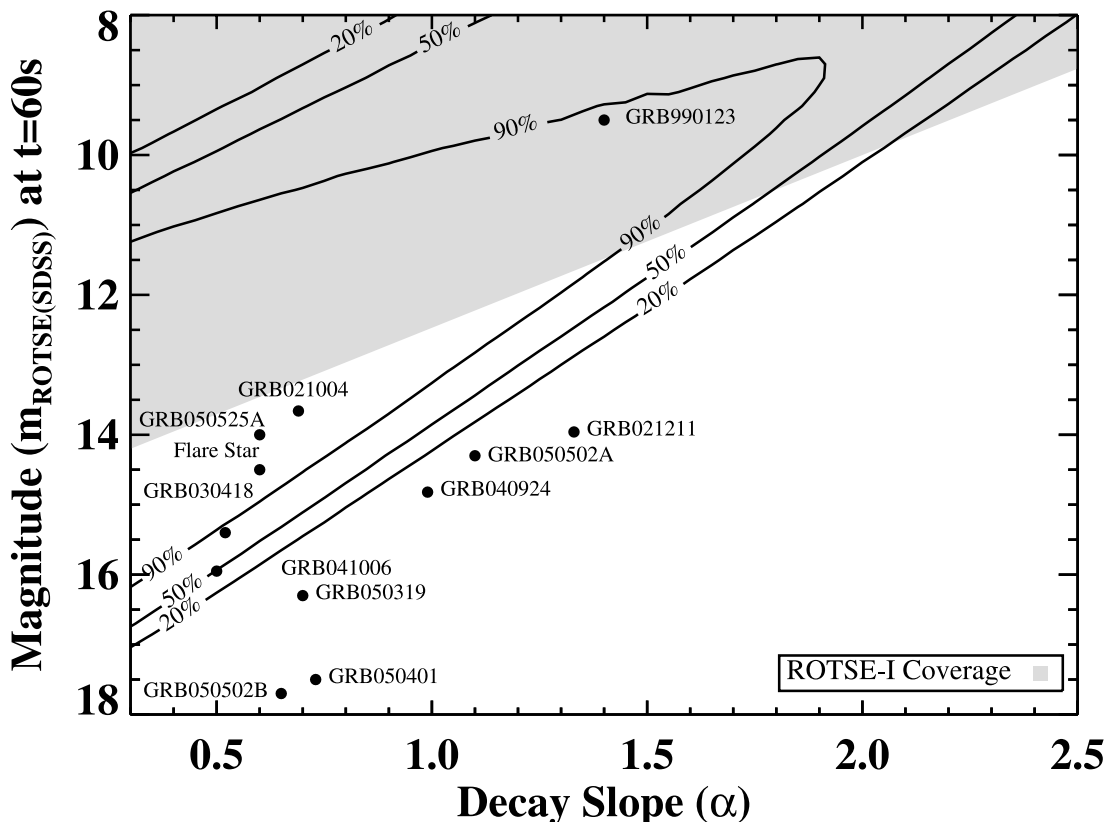

FIG. 5.—Detection efficiency for fading transients, parameterized by their peak magnitude at $t = t_0 + 60$ s, m_{60}, and their decay constant α. The efficiencies calculated assume 30 minutes of effective coverage for each set for an integrated coverage of 1.74 deg^2 yr. All sets with limiting magnitudes deeper than 17.5 were used for this plot. The contours describe our 20%, 50%, and 90% efficiency levels. The contours roll over at the bright end, where many transients would be saturated and rejected. The gray area describes the coverage in the ROTSE-I transient search. Overplotted are approximate peak magnitudes and decay constants (averaged over the first hour) for six GRB afterglows with early detections (Akerlof et al. 1999; Fox et al. 2003, 2004; Li et al. 2003; Rykoff et al. 2004b, 2005a, 2005b, 2005c; Yost et al. 2005; Falcone et al. 2005).

Figure 5 shows our detection efficiency for all the sets in the search with limiting magnitudes at the second epoch deeper than 17.5, assuming 30 minutes of coverage. The integrated coverage is 1.74 deg^2 yr for these sets. The 20%, 50%, and 90% contours are shown. The contour lines roll over at the bright end where our saturation cuts take effect—these extraordinarily bright transients would be vetoed in our pipeline. However, the ROTSE-I transient search covered much of this parameter space (*shaded area*) without finding any candidate afterglows with approximately twice as much coverage (Kehoe et al. 2002). Overplotted are approximate peak magnitudes and decay slopes, averaged over the first hour after the burst time, for 10 of the 12 GRB afterglows that have been detected in the first hour after the burst. The remaining two bursts are too faint to be placed on this plot. We are sensitive to ∼40% of these afterglows, which have been detected for ∼50% of all promptly localized GRBs. Also plotted is an inferred peak magnitude and decay slope for the flare star ROTSE3 J220806.9+023100.3, which is contained in the locus of afterglow points.

5. DISCUSSION

To date, this is the deepest wide-field search for untriggered and orphan GRBs. With a total coverage of 1.74 deg^2 yr, we have not found any candidate afterglows or other unknown transients. The primary reason we have been able to positively identify each of our transient candidates is the five-color SDSS data of the fields in our search. Other transient searches, such as the DLS, that can image much deeper do not have this advantage.

We have also determined that the backgrounds for a search of this type are purely astrophysical. We have not had any difficulty from satellite glints or any mysterious terrestrial flashes. Our primary background consists of asteroids with small proper motion, but the MPChecker database combined with follow-up observations can eliminate these. Outside the solar system, but within the Galaxy, we see a small but measurable rate of CVs and flare stars. The flare star ROTSE3 J220806.9+023100.3 is the only object that we have found that had a light curve that mimicked our expected signature of an untriggered GRB afterglow.

We can place an upper limit on the rate of fading optical transients with quiescent counterparts dimmer than ∼20th magnitude, as described by our 90% coverage region shown in Figure 5. To calculate an upper limit on the rate of transients in this region, we follow the method of Becker et al. (2004). The observed rate is

$$\eta = \frac{N}{\langle \mathcal{E} \rangle E} \ \text{events} \ \text{deg}^{-2} \ \text{yr}^{-1}, \qquad (1)$$

where N is the number of events, E is the exposure, and $\langle \mathcal{E} \rangle$ is the efficiency. With the observed number of transients $N_{\text{obs}} = 0$, Poisson statistics place an upper limit of $N_{\text{max}} < 3.0$ with 95% confidence. Therefore, we can place a 95% confidence upper limit of $\eta_{\text{max}} < 1.9 \ \text{deg}^{-2} \ \text{yr}^{-1}$ in our coverage region.

The launch of *Swift* will allow us to probe the early afterglow phase of GRBs far more systematically than has been achieved to date. We have learned some details from the variety of early afterglows detected so far. It is clear that very bright prompt

flashes like that from GRB 990123 (Akerlof et al. 1999) are not the norm. It also appears that extrapolating late-time afterglows to the early time generally overpredicts the brightness, as with GRB 030418 and GRB 030723 (Rykoff et al. 2004b). These data certainly make our search more difficult, as only ∼20% of GRBs have afterglows that fall within our sensitivity region.

If we assume that the γ-ray emission of GRBs is confined within a double jet with a cone half-angle of θ_{max}, while the optical emission is isotropic, then a given GRB is visible in a small fraction of the sky approximated by $\theta^2/2$. Therefore, the true rate of GRB events within the observable universe must be ∼$1500/\theta_{\text{max}}^2$ events yr^{-1}. The 95% confidence limit of $<78,000$ events yr^{-1} is for a region that is sensitive to ∼20% of GRBs, and therefore our assumption of isotropic optical emission is tenable as long as $\theta_{\text{max}} > 3°.6$. As this is an approximate estimate of the GRB jet angle, the present limits cannot set stringent bounds on the properties of these objects. However, if programs such as ours continue to reduce the upper bounds for the orphan afterglow rate, the isotropic emission hypothesis will become incompatible with what we know about the structure of GRB jets. Although this is not an enormous surprise, it does represent a sanity check of the accepted model of GRBs by completely independent reasoning.

Our search has also detected several previously unknown high Galactic latitude cataclysmic variables with dim quiescent counterparts. We have detected three new CVs with ∼52 deg^2 yr of coverage for slow decay transients that peak between 13th and 16th magnitude. This implies a rate of 0.06 deg^{-2} yr^{-1}. Assuming Poisson statistics, the 95% confidence upper limit on the rate is 0.17 deg^{-2} yr^{-1}. We have found one new CV with ∼25 deg^2 yr of coverage for CVs that peak between 16th and 18th magnitude. This implies a rate of 0.04 deg^{-2} yr^{-1}. Assuming Poisson statistics, the 95% confidence upper limit on the rate is 0.21 deg^{-2} yr^{-1}. If we extrapolate the rate over the whole sky, this would produce ∼2000 high Galactic latitude CV outbursts every year. In the "Living Edition" catalog of CVs there are only ∼130 CVs in our sensitivity range as of 2005 March (Downes et al. 2001). None of the CVs detected by ROTSE-III had been known previously. Our search results imply that many more CVs remain to be discovered.

The ROTSE-III transient search is an ongoing project. We expect to continue to patrol the sky over the lifetime of *Swift* (at least 2 years), as we wait for GRB triggers. We will thus gain another factor of 2–3 in coverage and will achieve a modest improvement toward the goal of ∼110 deg^2 yr, the threshold for having a high probability of finding an untriggered afterglow. In this paper, we have demonstrated that such a search is feasible, as the background rate of unknown transients is very low.

REFERENCES

Abazajian, K., et al. 2005, AJ, 129, 1755
Akerlof, C., et al. 1999, Nature, 398, 400
———. 2000, ApJ, 532, L25
———. 2003, PASP, 115, 132
Becker, A. C., et al. 2004, ApJ, 611, 418
Bertin, E., & Arnouts, S. 1996, A&AS, 117, 393

Downes, R. A., Webbink, R. F., Shara, M. M., Ritter, H., Kolb, U., & Duerbeck, H. W. 2001, PASP, 113, 764
Falcone, A., et al. 2005, GCN Circ. 3330, http://gcn.gsfc.nasa.gov/gcn/gcn3/3330.gcn3
Fenimore, E. E., et al. 1993, Nature, 366, 40
Fox, D. B. 2004, GCN Circ. 2741, http://gcn.gsfc.nasa.gov/gcn/gcn3/2741.gcn3

Fox, D. W., et al. 2003, Nature, 422, 284
Frail, D. A., et al. 2001, ApJ, 562, L55
Harrison, F. A., et al. 1999, ApJ, 523, L121
Kehoe, R., et al. 2001, ApJ, 554, L159
———. 2002, ApJ, 577, 845
Lamb, D. Q., et al. 2004, NewA Rev., 48, 423
Lasker, B. M., et al. 1998, BAAS, 30, 912
Li, W., Filippenko, A. V., Chornock, R., & Jha, S. 2003, ApJ, 586, L9
Monet, D. B. A., et al. 1998, VizieR Online Data Catalog, 1252, 0
Nakar, E., & Piran, T. 2003, NewA, 8, 141
Panaitescu, A., & Kumar, P. 2001, ApJ, 560, L49
Park, H. S., et al. 1999, A&AS, 138, 577
Rhoads, J. E. 1997, ApJ, 487, L1
Rykoff, E. 2005, ATel, 403, 1
Rykoff, E., & Quimby, R. 2005, ATel, 423, 1

Rykoff, E., Schaefer, B., & Quimby, R. 2005a, GCN Circ. 3116, http://gcn.gsfc.nasa.gov/gcn/gcn3/3116.gcn3
Rykoff, E. S., Yost, S. A., & Smith, D. A. 2005b, GCN Circ. 3165, http://gcn.gsfc.nasa.gov/gcn/gcn3/3165.gcn3
Rykoff, E. S., Yost, S. A., & Swan, H. 2005c, GCN Circ. 3465, http://gcn.gsfc.nasa.gov/gcn/gcn3/3465.gcn3
Rykoff, E. S., et al. 2004a, Inf. Bull. Variable Stars, 5559, 1
———. 2004b, ApJ, 601, 1013
Stanek, K. Z., Garnavich, P. M., Kaluzny, J., Pych, W., & Thompson, I. 1999, ApJ, 522, L39
Vanden Berk, D. E., et al. 2002, ApJ, 576, 673
Vestrand, W. T., et al. 2004, Astron. Nachr., 325, 549
Woudt, P. A., Warner, B., & Rykoff, E. 2005, IAU Circ., 8531, 3
Yost, S. A., Swan, H., Schaefer, B. A., & Alatalo, K. 2005, GCN Circ. 3322, http://gcn.gsfc.nasa.gov/gcn/gcn3/3322.gcn3